"Novel Drilling Technology Combining Hydro-Jet and Percussion for ROP Improvement in deep geothermal drilling"

This project has received funding from the European Union's Horizon 2020 research and innovation programme under grant agreement No 101006752

DELIVERABLE D6.4

"Modelling of hammer drilling and vibrations response for use of intensifier downhole"

ABSTRACT

This modelling study aimed at assisting the design and optimal use of a hybrid High Pressure Water-Jetting and percussive drilling (abbreviated as HPWJ-PD) system in which longitudinal stress waves propagating in the drill string are used to provide power to a downhole pressure intensifier.

A linear and a nonlinear model of a HPWJ-PD system were therefore established and applied. Both models treat the drill bit, the hammer, and the drill string as a rod system and describe the HPWJ intensifier as a mass-spring-damper (MSD) system. The linear model assumes a fixed boundary condition at the bit-rock interface, a linear damping coefficient along the rod system, and a linear damper inside the MSD. In contrast, the nonlinear model introduces a bi-linear bit-rock interface law, two different damping effect models (the Herschel–Bulkley and Casson models), and a nonlinear damper model obtained from the mechanism of the HPWJ intensifier. Scaling analyses of the two models are carried out to identify the key influencing parameters affecting the efficiency of energy harvesting. Results highlight the best optimization potential by acting on the frequency of the harmonic excitation (to be close to the natural frequency of the intensifier) and on the stiffness parameters of the bit-rock interface (loading-unloading stiffnesses, and the BRI-rod stiffness ratio).

DOCUMENT TYPE	Report
DOCUMENT NAME:	Modelling of hammer drilling and vibrations response for use of intensifier downhole
VERSION:	Vfinal
DATE:	23/01/2024
STATUS:	S0
DISSEMINATION LEVEL:	PU

Authors, Reviewers				
Author(s):	Xianfeng Song, Alexandre Kane, Stephane Dumoulin			
Affiliation(s):	SINTEF Industry			
Further Authors:				
Peer Reviewers:	Naveen Velmurugan (ARMINES)			
Review Approval:	Approved	Yes	Rejected (to be improved as indicated below)	
Remarks / Improvements:				

Version History			
Version:	Date:	Comments, changes, Status:	Person(s) / Organisation Short Name:
v0.1	25/12/23	First draft	Stéphane Dumoulin (SINTEF)
vfinal	23/01/24	Final version ready to submit	Naveen (ARMINES)

Version Numbering	
v0.x	draft before peer-review approval
v1.x	After the first review
v2.x	After the second review
vfinal	Deliverable ready to be submitted!

Status / Dissemination Level			
Status		Dissemination Level	
S0	Approved/Released/Ready to be submitted	**PU**	Public
S1	Reviewed	**CO**	Confidential, restricted under conditions set out in the Grant Agreement
S2	Pending for review		
S3	Draft for comments	**CI**	Classified, information as referred to in Commission Decision 2001/844/EC.
S4	Under preparation		

TABLE OF CONTENTS

1 Introduction 4
2 Linear Model 5
2.1 Mathematical Model 5
2.2 Simulation Results 7
2.2.1 Comparison between Different Approaches 7
2.3 Influence of the Excitation Frequency 8
2.4 Conclusions of the Section 9
3 Non-Linear Model 9
3.1 Mathematical Model 9
3.1.1 Overview of the Model 9
3.1.2 Dynamics of the System 10
3.1.3 Damping Force Models of the Drilling Fluid 12
3.1.4 Bit-Rock Interaction 13
3.1.5 Mechanism of the Intensifier 13
3.2 Simulation Results 15
3.2.1 Comparison between Two Damping Coefficient Models 15
3.2.2 Influence of the Bit-Rock Interface 17
3.3 Conclusions of the Section 18
4 Conclusions 19
References 19
Appendix A. HPWJ-PD linear model scaling 20
Appendix B. HPWJ-PD non-linear model scaling 22

CONTENT

1 Introduction

This deliverable 6.4 is addressing the dynamic response, at the macroscale level of the HPWJ-PD system, where the Bit-Rock-Interaction (BRI) response is recognized as the main source of nonlinearity and vibrations of the drilling structure.
Modelling developments were therefore done to enable a parametric study of the influence of drilling operating parameters, BRI response, and typical design parameters of hammer-intensifier system, on the longitudinal stress waves propagating in the drill string, which, in the hybrid HPWJ-PD system is harvested to provide power to a pressure intensifier.

Drilling (field) data measurements of Down-The-Hole hammer (DTH) was provided by Drillstar in 2021, which indicates small WOB and high frequency longitudinal frequencies that may lead to insufficient energy to activate a vibrational intensifier to produce the targeted water jet pressure of 150 MPa. In 2022, the applicability of the pressure intensifier was further investigated in a modelling study carried out by UPC (see deliverable 5.2: “Report on modelling, prediction and feasibility of the intensifier..”) which confirms that the WOB required for an efficient use of the pressure intensifier is significantly higher (by a factor 10) to the WOB conventionally used with DTH hammer. Pulse-shape and duration of vibration patterns were also unfavourable. Consequently, alternative downhole intensifier solutions have been prioritized (such as screw motor or electromagnetic valve control solutions) for the development of a HPWJ-PD demonstrator during the Orchyd project period.

Nevertheless, the modelling activities in deliverable 6.4 were carried out in order to investigate a wide range of parametric drilling configurations. This will allow a better understanding of the limit of applicability of such pressure intensifier, while paving the way for a more appropriate use where higher WOB can be applied, such as hybrid drilling technology combining rotary-percussive and water jet drilling.
Two models were thus established and applied in this study. The first model of the HPWJ-PD system is linear, as it simplifies the HPWJ module as a spring-mass-damping system connected to the drill string and the bit is treated as fixed point. Due to its linear nature, the response of this model to an harmonic force excitation can be calculated very efficiently using the matrix transfer method. Despite its simplicity, the model can highlight the critical role of the ratio of the loading frequency over the resonance frequency of the HPWJ module in harvesting energy from the drill string vibrations. Another utility of this model is to provide a benchmark for the semi-discretization method, which is used for computing the response of the nonlinear model.
The nonlinear model HPWJ-PD system departs from the linear ones in three aspects. First, the model of the HPWJ intensifier is modified by introducing a nonlinear damper to represent the expulsion of fluid from the intensifier. With this model, the pressure of the fluid jetted by the HPWJ can be estimated. Second, a bi-linear spring model is introduced to describe the bit-rock interaction in a more realistic way. Finally, two rheological models of the mud, Herschel–Bulkley and Casson, have been adopted to estimate the damping coefficient caused by the drilling mud. The parametric analysis to assess the influence of the controlling numbers on the response of the intensifier is reported, for each model, in the sections "simulation results".

2 Linear Model

2.1 Mathematical Model

The linear model of the hybrid HPWJ-PD system is sketched in Figure 1, where a fixed boundary condition is applied at the bit end and a damper is attached to the right end to represent the impedance matching boundary condition. A harmonic force $f(t) = F_0 sin(\omega_0 t)$ is applied at the interface between the bit and hammer assemblies, and the intensifier system is simplified as a mass-spring-damper (MSD) system attached to the rod with its distance from the hammer-bit interface L_2.

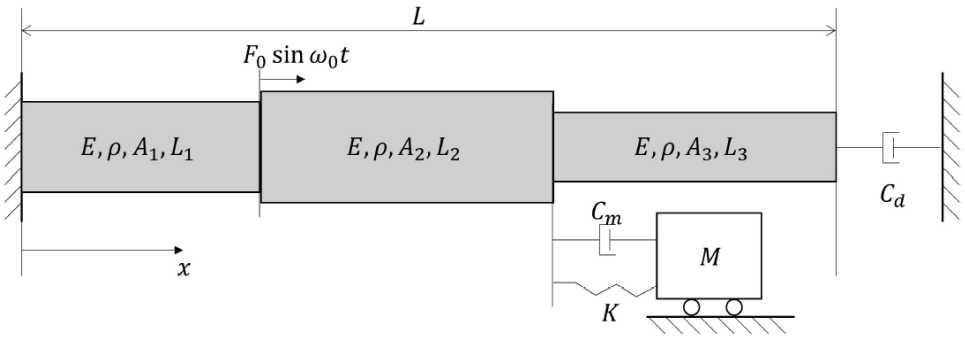

Figure 1: Schematic diagram of the hammer excitation and pressure intensifier system.

The axial dynamics of the rod is governed by a one-dimensional damped wave equation

$$\frac{\partial u^2(x,t)}{\partial t^2} + k_a \frac{\partial u(x,t)}{\partial t} - c^2 \frac{\partial u^2(x,t)}{\partial x^2} = 0, \tag{1}$$

where $u(x,t)$ represents the axial displacement of the rod at position $x \in [0, L]$ and time t, L is the rod total length, $c = \sqrt{\frac{E}{\rho}}$ is the axial wave velocity with E and ρ denoting, respectively, the Young's modulus and density of the rod material, k_a characterizes the axial viscous damping caused by the drilling mud.

According to Figure 1 the boundary conditions at $x = 0$ =and $x = L$ are given by

$$u(0,t) = 0, \tag{2}$$

$$EA_3 \frac{\partial u(L,t)}{\partial x} = -C_d \frac{\partial u(L,t)}{\partial t}, \tag{3}$$

where C_d is the damping value of the damper and impedance matching condition is applied when $C_d = A_3\rho c$.
The concentrated force at $x_1 = L_1$, representing the bit-hammer interaction, is expressed as

$$EA_1 \frac{\partial u}{\partial x}\Big|_{x=x_1^-} = EA_2 \frac{\partial u}{\partial x}\Big|_{x=x_1^+} + F_0 sin(\omega_0 t), \tag{4}$$

where L_1 is the length of the first rod segment, A_1 (A_2) are the cross-sectional area of the first (second) rod segment, F_0 and ω_0 are the amplitude and frequency of the harmonic excitation, respectively. Similarly, the concentrated force at x_1 = L_1 + L_2 exerted by the MSD system to the rod is given by:

$$EA_2 \frac{\partial u}{\partial x}\Big|_{x=x_2^-} = EA_3 \frac{\partial u}{\partial x}\Big|_{x=x_2^+} + K[U(t) - u(x_2, t] + C_m \left[\dot{U}(t) - \frac{\partial u(x_2,t)}{\partial t}\right], \tag{5}$$

where L_2 is the length of the second rod segment, A_3 is the cross-sectional area of third rod segment, K and C_m denote, respectively, the stiffness and damping of the MSD system, $U(t)$ is the axial displacement of the lumped mass M, and its motion is governed by an ordinary differential equation (ODE)

$$M\ddot{U}(t) + C_m \left[\dot{U}(t) - \frac{\partial u(x_2,t)}{\partial t}\right] + K[U(t) - u(x_2, t] = 0, \tag{6}$$

where the over-dot denotes derivative with respect to time. Note that displacement continuity conditions need to be satisfied at $x = x_1$ and $x = x_2$; they are given by

$$u(x_1^-, t) = u(x_1^+, t) = u(x_1, t), \tag{7}$$

$$u(x_2^-, t) = u(x_2^+, t) = u(x_2, t), \tag{8}$$

The system is initially at rest; hence the initial conditions are

$$u(0,t) = 0, \frac{\partial u(x,0)}{\partial t} = 0,\ U(0) = 0,\ \dot{U}(0) = 0, \tag{9}$$

Since the lumped mass is connected to the rod element via the spring and damper, we obtain a system of coupled partial differential equation (PDE) in (1) and ODE in (6). The set of coupled PDE-ODE with boundary conditions (2) - (5) and zero initial conditions (9) represents a closed system to simulate the dynamics of the advanced hammer-intensifier system.

To reduce the number of parameters in the coupled PDE-ODE system, the model was reformulated in a dimensionless form see Annex A. The rod-MSD (reformulated) model was first solved in the frequency domain using the transfer matrix method (with use of MATLAB), which is commonly used to solve the dynamic responses of a linear system with force or displacement input applied only at the system boundaries. The coupled system of PDE and ODE, was afterwards solved in the time domain using the semi-discretization method, in which the PDE is discretized into a system of ODEs numerically integrated using MATLAB.

2.2 Simulation Results

2.2.1 Comparison between Different Approaches

The values of dimensional and dimensionless parameters of the rod-intensifier system used in the simulation are listed, respectively, in Table 1 and Table 2, which are served as the benchmark values for parametric analysis. The time simulation results of the displacements at ξ = 1 and the lumped mass are presented in Figure 2, which show the harmonic variation of the displacement with the same frequency as the excitation frequency. Impedance matching boundary condition for ξ_d = 59.27 is used in the simulations. A transient response can be seen in the lumped mass displacement. However, the magnitude of the displacements in steady-states are 12.57 μm and 0,64 μm for the rod at ξ = 1 and lumped mass, respectively. The magnitude of displacements obtained using the transfer matrix method for the rod at ξ = 1 and lumped mass is 12.57 μm and 0,64 μm, which is exactly the same as those obtained in the time domain simulation.

Parameter	Values	Unit	Parameter	Value	Unit
K	2.6×10^5	N/s	E	210	GPa
M	1000	kg	ρ	8500	$\mathrm{kg/m^3}$
C_m	6000	Ns/m	F_0	10000	N
k_a	0.5	$\mathrm{s^{-1}}$	ω_0	40π	rad/s
L_1	6	m	A_1	0.0226	$\mathrm{m^2}$
L_2	6	m	A_2	0.0226	$\mathrm{m^2}$
L_3	6	m	A_3	0.0226	$\mathrm{m^2}$

Table 1: Benchmark values of dimensional parameters.

Parameter	Value	Parameter	Value
t_*	0.062 s	ζ_m	0.37
U_*	3.79×10^{-5} m	ζ_d	59.27
κ	17.13	ζ_a	0.031
η_0	7.79	ξ_1	0.33
β	1015	ξ_2	0.67
α_1	1	α_2	1

Table 2: Benchmark values of dimensionless parameters.

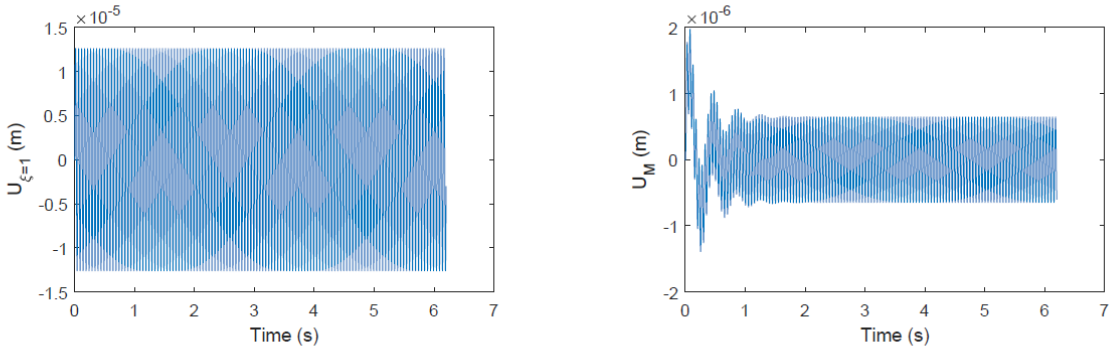

(a) (b)

Figure 2: Time simulation results of the displacement (a) at ξ = 1 and (b) the lumped mass.

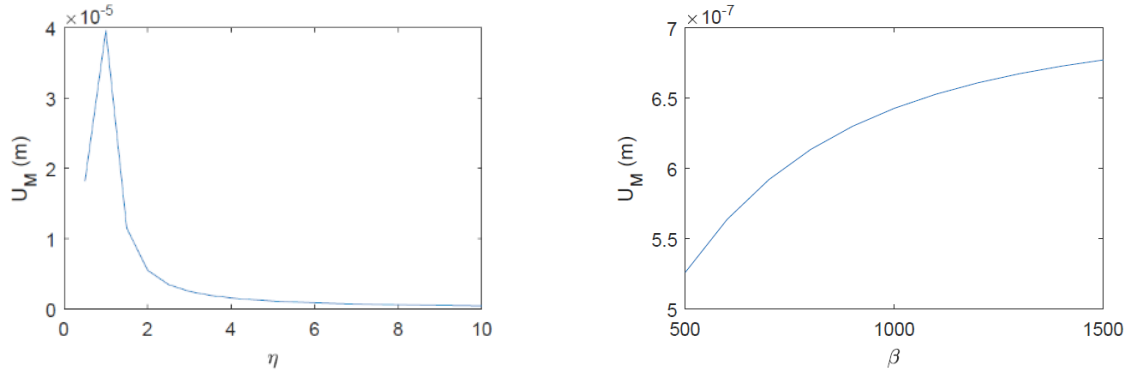

(a) (b)

Figure 3: Parametric studies of the influences of (a) η and (b) β on the lumped mass displacement.

2.3 Influence of the Excitation Frequency

Since the simulation results using the transfer matrix and the finite difference method are the same, the transfer matrix method is then used for parametric studies due to its computational efficiency. The influence of the excitation frequency η_0 and the stiffness ratio β on the intensifier displacement are shown in Figure 3 Figure 5. We can see from Figure 3a that the maximum displacement is achieved when the excitation frequency is the same as the natural frequency of the lumped mass. When the rod parameters remain unchanged, the variation of parameter $\beta = \frac{EA_1}{KL}$ reflects the change of the spring stiffness. We can thus infer from Figure 3b that decreasing the spring stiffness increases the intensifier displacement.

2.4 Conclusions of the Section

We have described a linear model of the hammer-intensifier system with a fixed boundary condition applied at the bit end and a damper attached to the right end to represent the impedance matching boundary condition. Furthermore, a harmonic force representing the interaction between the bit and hammer assembly is applied at the rod and the intensifier system simplified as a MSD system is attached to the rod. The dynamics of the rod is governed by a PDE, while the dynamics of the lumped mass is governed by an ODE, which is coupled with the PDE through the concentrated force associated to the MSD system. Scaling analysis of the model is carried out to reduce the number of parameters. This model is solved in the frequency domain using the transfer matrix method and in the time domain using the finite difference method. The simulation results using both approaches agree well with each other. On this basis, we studied the influence of the β and η on the axial displacement of the intensifier. As expected, the intensifier displacement achieves maximum value at the resonant frequency, but it decreases rapidly when the excitation frequency is larger than the resonant frequency. Also, the intensifier displacement increases gradually with increasing β, a number reflecting the compliance of the intensifier spring.

3 Non-Linear Model

This section describes a non-linear model of the hybrid HPWJ-PD system. Three key improvements have been made to the model presented in Sect. 2. First, a more detailed model of the HPWJ intensifier is constructed. With this model, the pressure inside the HPWJ, a key parameter determining whether the water jetted by the HPWJ can help break the rock, can be estimated. Second a bi-linear spring model is introduced to describe the bit-rock interaction in a more realistic way. Finally, two rheological models of the mud, Herschel–Bulkley and Casson, have been adopted to estimate the damping coefficient caused by the drilling mud.

3.1 Mathematical Model

3.1.1 Overview of the Model

Following Sect. 2.1, the drill bit, the hammer, and the drill string in the advanced HPWJ-PD model are modeled as three elastic rods, see Figure 4(a). A bi-linear spring representing the bit-rock interaction law is attached to the bit end, see Figure 4(b). In contrast, the impedance matching boundary condition is applied at the right end of the drill string, represented by a damper. The interaction between the bit and the hammer is simplified as a harmonic excitation $F_0 sin(\omega_0 t)$ exerted at the interface between the bit and the hammer. Finally, the HPWJ intensifier is simplified as a mass-spring-damper (MSD) system attached to the interface between the hammer and the drill string. A nonlinear damper is introduced to represent the expulsion of fluid from the pressure intensifier, see Figure 4(c).

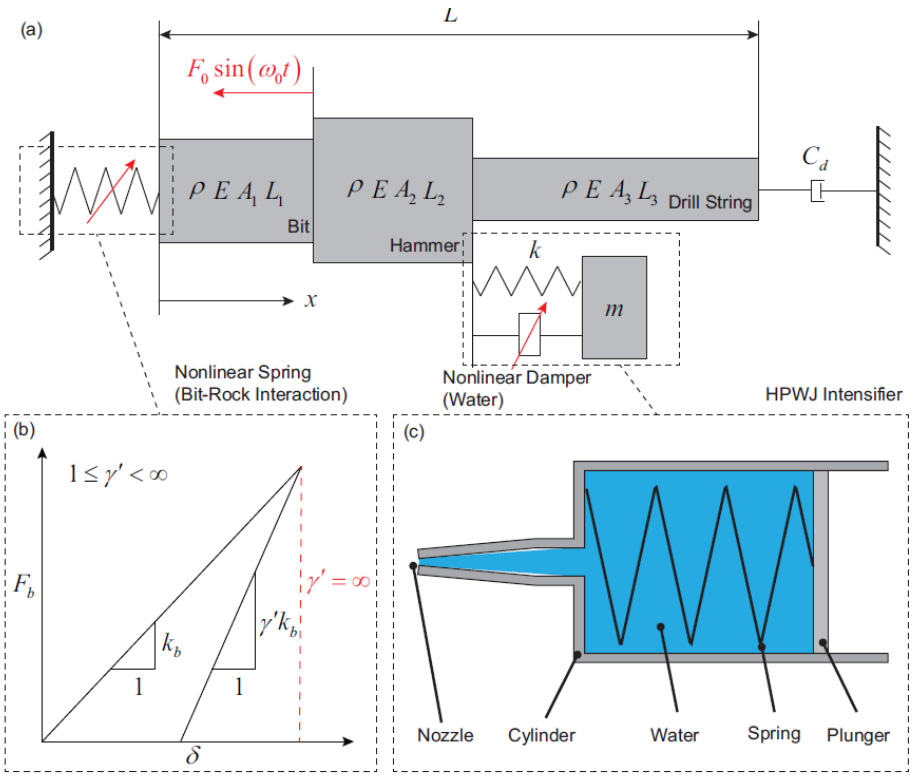

Figure 4: (a) Schematic diagram of the HPWJ-PD system. (b) Bi-linear bit-rock interaction law considering both loading and unloading processes. (c)

3.1.2 Dynamics of the System

Taking into account the nonlinear damping force $f_i(x,t)$ caused by the drilling fluid (see Sect. 3.1.3), the axial dynamics of the system is obtained as:

$$\frac{\partial u^2(x,t)}{\partial t^2} - c^2 \frac{\partial u^2(x,t)}{\partial x^2} + f_i(x,t) = 0, \quad i = 1,2,3. \tag{10}$$

The boundary conditions at $x = 0$ and $x = L$ are given respectively by

$$EA_1 \frac{\partial u(0,t)}{\partial x} + F_b = 0, \tag{11}$$

$$EA_3 \frac{\partial u(L,t)}{\partial x} = -C_d \frac{\partial u(L,t)}{\partial t}, \tag{12}$$

where F_b is the bit-rock interaction force, see Sect. 3.1.4. The concentrated force at $x_1 = L_1$, representing the bit-hammer interaction, is expressed as

$$EA_1 \frac{\partial u}{\partial x}\Big|_{x=x_1^-} = EA_2 \frac{\partial u}{\partial x}\Big|_{x=x_1^+} - F_0 sin(\omega_0 t), \tag{13}$$

Similarly, the concentrated force at $x_2 = L_1 + L_2$ exerted by the HPWJ intensifier to the rod is given by

$$EA_2 \frac{\partial u}{\partial x}\Big|_{x=x_2^-} + F_{int}| = EA_3 \frac{\partial u}{\partial x}\Big|_{x=x_2^+} + K[U(t) - u(x_2, t], \tag{14}$$

The motion of the plunger is governed by the following ODE:

$$M\ddot{U}(t) + K[U(t) - u(x_2, t] = F_{int} \tag{15}$$

where F_{int} is the nonlinear damping force introduced by the intensifier, which is discussed in Sect. 3.1.5. The displacement continuity conditions need to be satisfied at $x = x_1$ and $x = x_2$; they are given by:

$$u(x_1^-, t) = u(x_1^+, t) = u(x_1, t), \tag{16}$$

$$u(x_2^-, t) = u(x_2^+, t) = u(x_2, t), \tag{17}$$

The system is initially at rest; hence the initial conditions are

$$u(0, t) = 0, \frac{\partial u(x,0)}{\partial t} = 0,\ U(0) = 0,\ \dot{U}(0) = 0, \tag{18}$$

3.1.3 Damping Force Models of the Drilling Fluid

In this section, two different models are introduced to describe the damping force $f_i(x,t)$ caused by the drilling fluid. The simulation results with the two models are then compared to evaluate their influences on the efficiency of energy harvesting.

To begin with, according to the Herschel–Bulkley model [1], the damping force $f_i(x,t)$ is given by:

$$f_i(x,t) = \frac{\pi D_i}{\rho A_i}\left(\tau_{Hy} + k_f \frac{v^m}{\Delta_i^m}\right) sgn(v), \quad 1 = 1,2,3, \tag{19}$$

where the index i is determined by:

$$i = \begin{cases} 1 & 0 < x < x_1 \\ 2 & x_1 < x < x_2, \\ 3 & x_2 < x < x_3 \end{cases} \tag{20}$$

and $sgn(v)$is the sign function:

$$sgn(v) = \begin{cases} 1 & v > 0 \\ 0 & v = 0, \\ -1 & v < 0 \end{cases} \tag{21}$$

with $v = \frac{\partial u(x,t)}{\partial t}$ denotes the rod velocity.

For the sake of simplicity, the drill bit, the hammer, and the drill string are all modeled as circular hollow cylinders with D_1, D_2, and D_3 denoting their outer diameters, respectively. In (19) $\tau_{Hy} \in [3,7]$ (Pa) is the Herschel–Bulkley yield stress; $k_f \in [0,5]$ (Pa.s^m) is the fluid consistency index; $m \in [0,1]$ is the power-law exponent. In equation (19), Δ_i is the thickness of the mud layer:

$$\Delta_i = \frac{D_w - D_i}{2}, \quad 1 = 1,2,3, \tag{22}$$

where D_w is the inner diameter of the wellbore.

In contrast, according to the Casson rheological model [1], the damping force $f_i(x,t)$ is determined by:

$$f_i(x,t) = \frac{\pi D_i}{\rho A_i}\left(\tau_{Cy} + \mu\frac{v}{\Delta_i} + 2\sqrt{\mu\tau_{Cy}\frac{v}{\Delta_i}}\right)sgn(v), \quad 1 = 1,2,3, \tag{23}$$

where $\tau_{Cy} \in [0{,}14]$ (Pa) is the Casson yield stress and $\mu \in [0{,}1]$ (Pa.s) is the Casson plastic viscosity.

3.1.4 Bit-Rock Interaction

According to the experimental data in [2][3], the bit-rock interaction in PD can be described by a bi-linear spring model illustrated in Figure 4(b).

$$F_b = \begin{cases} k_b\delta, & \delta > 0,\ \dot{\delta} > 0 \\ k_b\delta_m + \gamma' k_b(\delta - \delta_m) = 0, & \delta > 0, \dot{\delta} < 0, \\ 0, & \delta < 0, \end{cases} \tag{24}$$

where F_b is the force interaction between the drill bit and rock; δ is the penetration of the bit; and m is the maximum penetration in the loading process. In the loading process ($\delta > 0,\ \dot{\delta} > 0$), the stiffness of the spring is k_b. In contrast, this stiffness changes to $\gamma' k_b$ in the unloading process ($\delta > 0,\ \dot{\delta} < 0$). When the penetration $\delta < 0$, the bit loses contact with the rock and the interaction force is zero. It is noted that the penetration δ can be determined by the displacement at the left end the drill bit:

$$\delta = -u(0,t). \tag{25}$$

3.1.5 Mechanism of the Intensifier

In (15), the nonlinear damping force $f_{int}(t)$ is caused by the fluid inside the intensifier, see Figure 4(c).

$$f_{int}(t) = p(t)A. \tag{26}$$

where $p(t)$ is the pressure of the fluid inside the HPWJ intensifier and A is the cross-sectional area of the intensifier. Here the pressure of the fluid inside the HPWJ $p(t)$ is assumed to be that of the fluid at the plunger.

By ignoring the gravity and by viewing the fluid inside the HPWJ as an ideal fluid - a fluid that is incompressible and has no viscosity, the fluid flow inside the HPWJ is governed by the Bernoulli's equation:

$$p(t) + \frac{\rho_w v_p^2}{2} = p_n + \frac{\rho_w v_n^2}{2}, \tag{27}$$

where ρ_w is the density of the fluid. p_n and v_n are the pressure and the velocity of the fluid at the nozzle. v_p is the relative velocity between the plunger and the cylinder of the HPWJ fixed to the rod system:

$$v_p = \frac{\partial u(x_2,t)}{\partial t} - \dot{U}(t), \tag{28}$$

It is noted that the intensifying process occurs when $v_p > 0$.

At the nozzle, the flow rate of the fluid is determined through

$$Q = A_n v_n, \tag{29}$$

Where A_n is the cross-sectional area of the outlet of the nozzle. For an incompressible fluid, the same flow rate can also be calculated at the cross-section under the plunger:

$$Q = A v_p. \tag{30}$$

Substitute (29) and (30) into (31), we have:

$$p(t) - p_n = \frac{\rho_w\left[\left(\frac{A}{A_n}\right)^2 - 1\right] v_p^2}{2}, \tag{31}$$

Given that $A \gg A_n$ ($\frac{A}{A_n} \gg 1$), (31) is simplified to

$$p(t) - p_n \approx \frac{\rho_w\left(\frac{A}{A_n}\right)^2 v_p^2}{2}, \tag{32}$$

According to [4], the pressure at the outlet of the nozzle is set to p_n, which results in

$$p(t) \approx \frac{\rho_w \left(\frac{A}{A_n}\right)^2 v_p^2}{2}, \tag{33}$$

For the case v_p < 0, the pressure $p(t)$ is artificially set to zero for the sake of simplicity. In summary we have

$$p(t) = \begin{cases} \frac{\rho_w \left(\frac{A}{A_n}\right)^2 v_p^2}{2} & v_p > 0 \\ 0 & v_p \leq 0 \end{cases}, \tag{34}$$

The term $f_{int}(t) = p(t)A$ can be viewed as a nonlinear damper in (14) and (15). Moreover, the pressure $p(t)$ is also a key parameter evaluating whether or not the water jetted by the intensifier can help break the rock. Similar to Sect. 2.1, we obtained a system of coupled PDE-ODE with boundary conditions (11) - (14) and zero initial conditions (18), representing a closed system to simulate the dynamics of the advanced HPWJ-PD system.

To reduce the number of parameters in the coupled PDE-ODE system, the model is reformulated in a dimensionless form see Annex B. The reformulated coupled PDE-ODE system was solved using a semi-discretization method, where the PDE is discretized into a system of ODEs. The entire system of ODEs was numerically integrated in MATLAB using the Runge-Kutta method.

3.2 Simulation Results

3.2.1 Comparison between Two Damping Coefficient Models

The values of dimensional parameters of the rod-intensifier system used in the simulation are listed in Table 3, which serve as the benchmark values for parametric analysis. Figure 5 illustrates the movement of the plunger of the HPWJ intensifier predicted using the Herschel–Bulkley model (τ_{Hy} = 5 Pa, m = 0.5, and k_f = 2.5 Pa.s^m) and the Casson model (τ_{Cy}= 7 Pa and μ = 0.5 Pa.s). The transient responses of the plunger simulated by the two models agree well with each other. Both of them are decreasing because of the damping effect of the fluid inside the HPWJ, and their frequencies are both close to the natural frequency of the MSD. In contrast, the steady state responses predicted by the two models are different. However, both of them are one order of magnitude smaller than the transient responses. This is because the frequency of the excitation is much higher than the natural frequency of the HPWJ intensifier. In this case, the damping effect of the drilling mud is not a key factor that affects the amplitude of the vibration of the HPWJ intensifier. The proposed statement is further convinced by a parametric analysis. As shown in Figure 6(a-e), neither the selection of damping coefficient models nor the parameters used in these models show a remarkable influence on the pressure inside the HPWJ intensifier, In contrast, the pressure of the intensifier is significantly affected

by the dimensionless parameter $\eta_0 = \omega_0 t^* = \omega_0\sqrt{\frac{M}{K}}$, see Figure 6(f), and the best performance is achieved when η_0 is close to 1. Physically, η_0 is the ratio between the frequency of the harmonic excitation (f_e) and the natural frequency of the intensifier (f_n):

$$f_c = \frac{\omega_0}{2\pi}, \qquad f_n = \frac{1}{2\pi}\sqrt{\frac{K}{M}}, \qquad \eta_0 = \omega_0\sqrt{\frac{M}{K}} = \frac{f_c}{f_n} \tag{35}$$

When and only when the frequency of the harmonic excitation is close to the natural frequency of the intensifier, the intensifier is fully "excited" and the vibration energy of the drill string can be efficiently harvested.

Parameter	Values	Unit	Parameter	Value	Unit
K	2.5×10^6	N/m	M	7000	kg
A	0.0024	m^2	A_n	3×10^{-6}	m^2
ρ_w	1000	kg/m^3	ρ	8500	kg/m^3
E	210	GPa	τ_{Hy}	[3, 7]	Pa
k_f	[0, 5]	$Pa \cdot s^m$	m	[0, 1]	-
τ_{Cy}	[0, 14]	Pa	μ	[0, 1]	$Pa \cdot s$
F_0	10000	N	ω_0	40π	rad/s
D_1	0.206	m	ID_1	0	m
D_2	0.206	m	ID_2	0	m
D_3	0.18	m	ID_3	0.06	m
D_w	0.216	m	L_1	10	m
L_2	10	m	L_3	180	m
k_b	3×10^7	N/m	γ'	4	-

Table 3: Benchmark values of dimensional parameters.

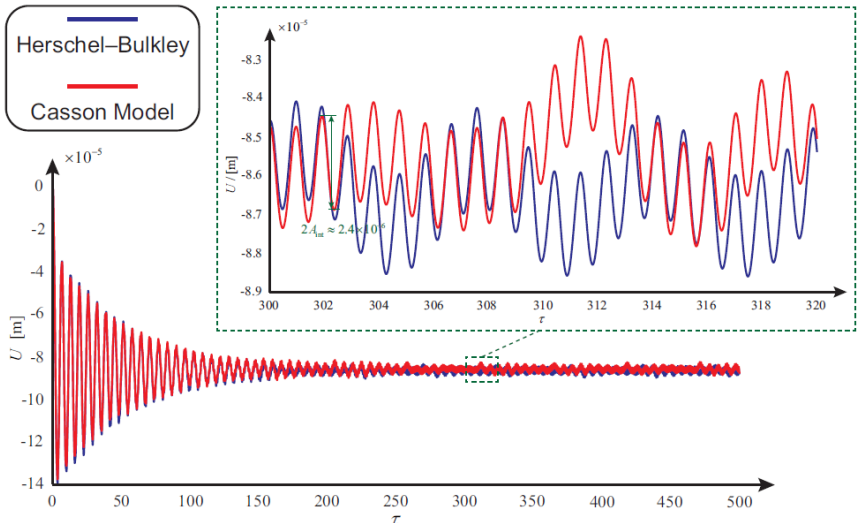

Figure 5: Displacement of the plunger as a function of scaled time τ, simulated using the Herschel–Bulkley model (τ_{Hy} = 5 Pa, m = 0.5, and k_f = 2.5 Pa.s^m) and the Casson model (τ_{Cy}= 7Pa and μ = 0.5 Pa.s).

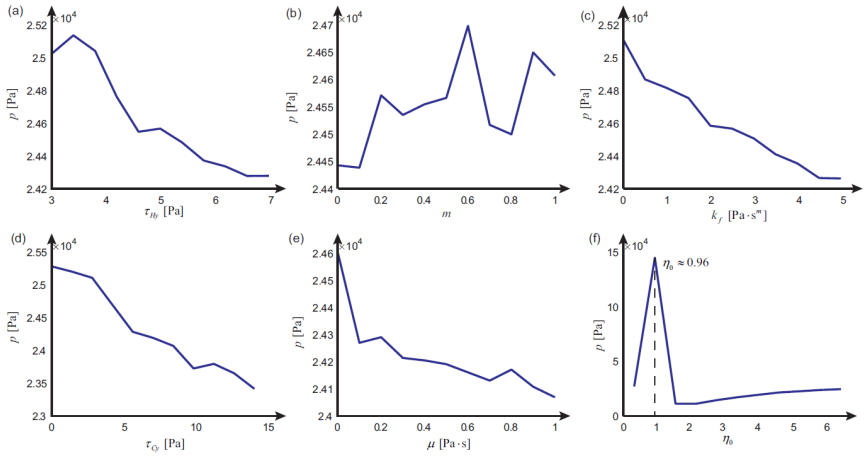

Figure 6: The influence of several factors on the maximum pressure inside the HPWJ intensifier: Herschel–Bulkley model parameters (a) τ_{Hy} , (b) m, and (c) k_f ; Casson model parameters (d) τ_{Cy} and (e) μ; and the dimensionless parameter η_0.

3.2.2 Influence of the Bit-Rock Interface

In this section the influences of the bit-rock interface parameters (β_b and γ') on the efficiency of the intensifier are analysed. Broadly speaking, the maximum pressure increase p_m inside the HPWJ intensifier decreases as the dimensionless parameter β_b increases, see Figure 7. Here $\beta_b = k_b L/EA_1$ describes the ratio between the stiffness of the bit-rock interface and that of the drill string. The highest pressure increase is obtained when β_b = 0, because there is no energy dissipation if the bit-rock interface is removed.

Meanwhile. the maximum pressure inside the intensifier also decreases when the parameter γ' increases, see Figure 8. This can be explained from the loading-unloading loop of the bi-linear spring. As illustrated in Figure 9 the triangle formed by the loading process, the unloading process, and the δ-axis reflects the energy dissipation in one loop. The area of this triangle increases when γ' increases, therefore more energy are dissipated and the pressure inside the intensifier decreases

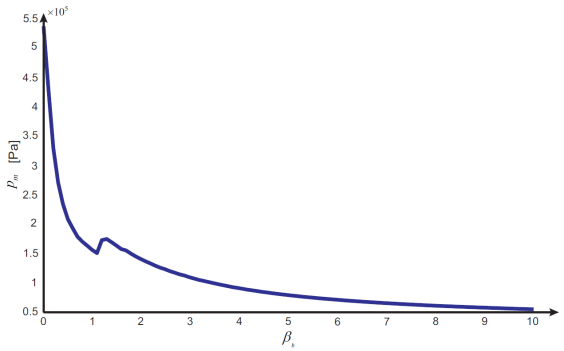

Figure 7: The maximum pressure increase p_m as a function of β_b (γ' = 4).

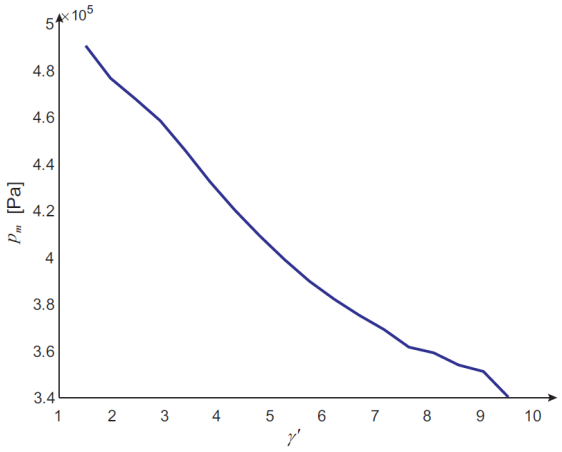

Figure 8: The maximum pressure increase p_m as a function of γ' (β_b = 0.1).

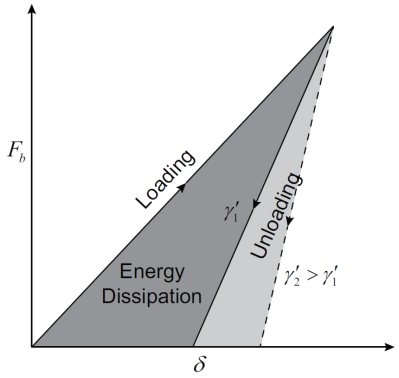

Figure 9: Energy dissipation in the loading-unloading loop of the bi-linear spring.

3.3 Conclusions of the Section

An advanced non-linear model of the hybrid HPWJ-PD system was provided, where three key improvements have been made over the linear model introduced in Sect. (2). First, the Herschel–Bulkley and Casson models were used to describe the damping effect of the drilling mud. Second, a bi-linear spring model was introduced to describe the bit-rock interaction in the percussive drilling process. Finally, the mechanism of the HPWJ intensifier was analysed using fluid dynamics (the Bernoulli's equation), through which the pressure of the fluid inside the intensifier can be estimated. By coupling a PDE governing the dynamics of the drill string and an ODE governing the dynamics of the intensifier, a PDE-ODE model was established to describe dynamics behavior of the HPWJ-PD system. Scaling analysis of the model was carried out to identify the key influencing parameters, and a semi-discretization method was adopted to solve the scaled model numerically. Parametric analysis shown that the key factor affecting performance of the HPWJ intensifier is the ratio of the frequency of the harmonic hammer excitation and the natural frequency of the intensifier, and the best performance is achieved when this ratio is close to one. Moreover, the influences of dimensionless bit-rock interface parameters β_b and γ' on maximum pressure increase p_m inside the intensifier were analysed. Simulation results shown that the efficiency of energy harvesting decreases as β_b and γ' increases.

4 Conclusions

This report has described a linear and a nonlinear model of a hybrid High Pressure Water-Jetting (HPWJ) and percussive drilling (PD) system. Both models treat the drill bit, the hammer, and the drill string as a rod system and describe the HPWJ intensifier as a mass-spring-damper (MSD) system. The linear model assumes a fixed boundary condition at the bit-rock interface, a linear damping coefficient along the rod system, and a linear damper inside the MSD. In contrast, the nonlinear model introduces a bi-linear bit-rock interface law, two different damping effect models (the Herschel–Bulkley and Casson models), and a nonlinear damper model obtained from the mechanism of the HPWJ intensifier. By coupling a PDE governing the dynamics of the rod and an ODE governing the dynamics of the MSD, both linear and non-linear models are described by a PDE-ODE system. Scaling analysis of the two models are carried out to identify the key influencing parameters, and a semi-discretization method is adopted to solve, in the time domain, the scaled models numerically. The linear model is also analysed in the frequency domain using the Transfer Matrix Method, whose results are consistent those simulated in the time domain and demonstrate the reliability of the semi-discretization algorithm. A parametric analysis has identified the following two groups of dimensionless parameters affecting the efficiency of energy harvesting.

- Dimensionless parameters associated with the structural design: (i) η_0 the ratio between the frequency of the harmonic excitation and the natural frequency of the intensifier (MSD) and (ii) β the ratio between the rod stiffness and the spring stiffness in the MSD. The best performance is achieved when this ratio η_0 is close to one and the efficiency of energy harvesting increases as β increases.

- Dimensionless parameters associated with the bit-rock interface: (i) β_b the ratio between the stiffness of the bit-rock interface and that of the rod and (ii) γ' the ratio between the stiffness of the bit-rock interface in the loading process and that in the unloading process. The efficiency of energy harvesting decreases as β_b and γ' increase.

References

[1] Agata Guzek, Igor Shufrin, Elena Pasternak, and Arcady V Dyskin. Influence of drilling mud rheology on the reduction of vertical vibrations in deep rotary drilling. Journal of Petroleum Science and Engineering, 135:375–383, 2015.

[2] WA Hustrulid and C Fairhurst. A theoretical and experimental study of the percussive drilling of rock part iii experimental verification of the mathematical theory. In International Journal of Rock Mechanics and Mining Sciences & Geomechanics Abstracts, volume 9, pages 417–418. Elsevier, 1972.

[3] Xianfeng Song, Ole Morten Aamo, Pascal-Alexandre Kane, and Emmanuel Detournay. Influence of weight-on-bit on percussive drilling performance. Rock Mechanics and Rock Engineering, 54(7):3491– 3505, 2021.

[4] Huajian Wang, Hualin Liao, Jun Wei, Yongwang Liu, Wenlong Niu, John-Paul Latham, Jiansheng Xiang, Jiansheng Liu, and Jingkai Chen. Pressure Drop Model and Jet Features of Ultra High Pressure Water Jet for Downhole Intensifier. Journal of Energy Resources Technology, 144(12), 05 2022. 123005.

Appendix A. HPWJ-PD linear model scaling

To reduce the number of parameters in the coupled PDE-ODE system, the model is reformulated in a dimensionless form by introducing scales for length (L_*), time (t_*), force (F_*), and displacement (U_*). Here we choose

$$L_* = L,\ t_* = \sqrt{\frac{M}{K}},\quad F_* = F_0,\quad U_* = \frac{F_0 L}{EA_1}. \tag{36}$$

where L_* is the total length of the rod, t_* is proportional to the period of free vibrations of the spring-mass system, F_* is amplitude of the force excitation, and U_* is and the change of length of the rod under the static load F_*. With these scales, we can define the following dimensionless variables.

$$\xi = \frac{x}{L},\quad \tau = \frac{u(x,t)}{U_*},\quad \overline{u}(\xi,\tau) = \frac{u(x,t)}{U_*},\quad \overline{U}(\tau) = \frac{U(t)}{U_*},$$
$$\overline{F}(\xi,\tau) = \frac{F(x,t)}{F_0},\quad \overline{P}(\tau) = \frac{P(t)}{F_0}, \tag{37}$$

where $\overline{u}(\xi,\tau)$ and $\overline{F}(\xi,\tau)$) are the displacement and force associated with the rod, respectively; $\overline{U}(\tau)$ and $\overline{P}(\tau)$ are the displacement and force associated with the MSD system, respectively. Hence, the set of coupled PDE-ODE can be reformulated in a dimensionless form as

$$\frac{\partial^2 \overline{u}}{\partial \tau^2} + \zeta_a \frac{\partial \overline{u}}{\partial \tau} - \kappa^2 \frac{\partial^2 \overline{u}}{\partial \xi^2} = 0 \tag{38}$$

$$\ddot{U} + \zeta_m \left[\dot{U} - \frac{\partial \overline{u}(\xi_2,\tau)}{\partial \tau}\right] + \left[\overline{U} - \overline{u}(\xi_2,\tau)\right] = 0 \tag{39}$$

where $\kappa = \frac{ct_*}{L}$ is the ratio of the wavelength over the total rod length, $\zeta_a = k_a t_*$ is the dimensionless viscous damping coefficient, and $\zeta_m = \frac{C_m t_*}{M}$ is the dimensionless damping coefficient of the damper of MSD system. The scaled boundary/interface conditions for the rod-MSD system read

$$\overline{u}(0,\tau) = 0, \tag{40}$$

$$\left.\frac{\partial \overline{u}}{\partial \xi}\right|_{\xi=\xi_1^-} = \alpha_1 \left.\frac{\partial \overline{u}}{\partial \xi}\right|_{\xi=\xi_1^+} + \ sin(\eta_0 \tau), \tag{41}$$

$$\left.\frac{\partial \overline{u}}{\partial \xi}\right|_{\xi=\xi_2^-} = \alpha_2 \left.\frac{\partial \overline{u}}{\partial \xi}\right|_{\xi=\xi_2^+} + \frac{1}{\alpha_1 \beta}\left[\overline{U} - \overline{u}(\xi_2,\tau)\right] + \frac{\zeta_m}{\alpha_1 \beta}\left[\dot{\overline{U}} - \frac{\partial \overline{u}(\xi_2,\tau)}{\partial \tau}\right], \tag{42}$$

$$\left.\frac{\partial \overline{u}}{\partial \xi}\right|_{\xi=1} = -\frac{\zeta_d}{\alpha_1 \alpha_2 \beta} \left.\frac{\partial \overline{u}}{\partial \tau}\right|_{\xi=1}, \tag{43}$$

where $\alpha_1 = \frac{A_1}{A_2}$ and $\alpha_2 = \frac{A_2}{A_3}$ are the ratios of different rod cross sectional area, $\eta_0 = \omega_0 t^*$ is the dimensionless excitation frequency, $\beta = \frac{EA_1}{KL}$ is the ratio between rod stiffness and spring stiffness, $\zeta_d = \frac{C_d t^*}{K}$ is the dimensionless damping coefficient of the damper attached to the rod. The scaled continuity and initial conditions are given by

$$\overline{u}(\xi_1^-,\tau) = \overline{u}(\xi_1^+,\tau) = \overline{u}(\xi_1,\tau) \tag{44}$$

$$\overline{u}(\xi_2^-,\tau) = \overline{u}(\xi_2^+,\tau) = \overline{u}(\xi_2,\tau) \tag{45}$$

$$\overline{u}(\xi,\tau) = 0, \qquad \frac{\partial \overline{u}(x,0)}{\partial t} = 0, \qquad \overline{U}(0) = 0, \qquad \dot{\overline{U}}(0) = 0 \tag{46}$$

Appendix B. HPWJ-PD non-linear model scaling

In this section, scaling is conducted using the same scales described in Appendix A, and the following additional dimensionless variables are introduced:

$$\overline{f_i}(\xi,\tau) = \frac{f_i(x,t)t_*^2}{U_*}, \qquad \overline{F}_{int} = \frac{F_{int}}{F_*}, \qquad \overline{F}_b = \frac{F_b}{F_*}. \tag{47}$$

where $\overline{f_i}(\xi,\tau)$ is the scaled damping term along the rod system, F_{int} is the scaled damping force of the intensifier and $\overline{F}_b$ is the scaled cutting force.

Hence, the set of coupled PDE-ODE can be reformulated in a dimensionless form as

$$\frac{\partial^2\overline{u}}{\partial\tau^2} - \kappa^2\frac{\partial^2\overline{u}}{\partial\xi^2} + \overline{f_i}(\xi,\tau) = 0, \tag{48}$$

$$\ddot{\overline{U}} + [\overline{U} - \overline{u}(\xi_2,\tau)] = \beta\overline{F}_{int}. \tag{49}$$

where κ and β are numbers:

$$\kappa = \frac{ct_*}{L}, \qquad \beta = \frac{F_*}{KU_*}. \tag{50}$$

In fact, κ and β can be viewed as ratios of scales. To begin with, the time and length scales associated with the MSD system (ODE) are

$$t_*^m = \sqrt{\frac{M}{K}}, \qquad l_*^m = \frac{F_*}{K}. \tag{51}$$

In contrast, the time and length scales associated with the rod system (PDE) are

$$t_*^r = \frac{L}{c}, \qquad l_*^r = \frac{F_* L}{E A_1}. \tag{52}$$

In this report, t_*^m and l_*^r are selected as the "hybrid" time and length scales of the PDE-ODE system, i.e., $t_* = t_*^m$and $U_* = l_*^r$. From this perspective, κ can be viewed as the ratio of the time scale associated with the ODE system over that associated with the PDE system, and β is the ratio of the ODE time scale t_*^m over that of the PDE length scale l_*^r :

$$\kappa = \frac{t_*^m}{t_*^r}, \qquad \beta = \frac{l_*^m}{l_*^r} \tag{53}$$

While using the Herschel–Bulkley model, the scaled damping term in (48) reads

$$\frac{\partial^2 \overline{u}}{\partial \tau^2} - \kappa^2 \frac{\partial^2 \overline{u}}{\partial \xi^2} + \overline{f_i}(\xi, \tau) = 0, \tag{54}$$

$$\bar{f}_i(\xi, \tau) = \left[\bar{\tau}_{Hi} + \bar{\kappa}_{fi} \dot{\bar{u}}^m\right] sgn(\dot{\bar{u}}), \qquad i = 1, 2, 3, \tag{55}$$

where $\dot{\bar{u}} = \frac{\partial \overline{u}}{\partial \tau}$, and $\bar{\tau}_{Hi}$ and $\bar{\kappa}_{fi}$ are dimensionless scalars

$$\bar{\tau}_{Hi} = \frac{\pi D_i t_*^2 \tau_{Hy}}{\rho A_i U_*}, \qquad \bar{\kappa}_{fi} = \frac{\pi D_i t_*^{2-m} k_f}{\rho A_i U_*^{1-m} \Delta_i^m}. \tag{56}$$

While using the Casson model, the scaled damping term becomes

$$\bar{f}_i(\xi, \tau) = \left[\bar{\tau}_{Ci} + \bar{\mu}_i \dot{\bar{u}} + 2\sqrt{\bar{\tau}_{Ci} \bar{\mu}_i} \sqrt{\dot{\bar{u}}}\right] sgn(\dot{\bar{u}}), \qquad i = 1, 2, 3, \tag{57}$$

where $\bar{\tau}_{Ci}$, $\bar{\mu}_i$ and ζ are dimensionless scalars

$$\bar{\tau}_{Ci} = \frac{\pi D_i t_*^2 \tau_{Cy}}{\rho A_i U_*}, \qquad \bar{\mu}_i = \frac{\pi D_i t_* \mu}{\rho A_i \Delta_i}. \tag{58}$$

The scaled damping force of the intensifier in (49) is

$$\overline{F}_{int} = \begin{cases} \varepsilon \left[\frac{\partial \overline{u}(\xi_2,t)}{\partial \tau} - \dot{\bar{U}}(t) \right]^2 & \frac{\partial \overline{u}(\xi_2,t)}{\partial \tau} - \dot{\bar{U}}(t) > 0 \\ 0 & \frac{\partial \overline{u}(\xi_2,t)}{\partial \tau} - \dot{\bar{U}}(t) \le 0 \end{cases}, \tag{59}$$

$$\varepsilon = \frac{\rho_\omega A^3 U_*^2}{2 A_n^2 F_* t_*^2} \tag{60}$$

The scaled boundary/interface conditions for the rod-MSD system read

$$\frac{\partial \overline{u}(0,\tau)}{\partial \xi} + \overline{F}_b = 0, \tag{61}$$

$$\left. \frac{\partial \overline{u}}{\partial \xi} \right|_{\xi=\xi_1^-} = \alpha_1 \left. \frac{\partial \overline{u}}{\partial \xi} \right|_{\xi=\xi_1^+} - \sin(\eta_0 \tau), \tag{62}$$

$$\left. \frac{\partial \overline{u}}{\partial \xi} \right|_{\xi=\xi_2^-} + \frac{1}{\alpha_1} \overline{F}_{int} = \alpha_2 \left. \frac{\partial \overline{u}}{\partial \xi} \right|_{\xi=\xi_2^+} + \frac{1}{\alpha_1 \beta} \left[\overline{U} - \overline{u}(\xi_2,\tau) \right], \tag{63}$$

$$\left. \frac{\partial \overline{u}}{\partial \xi} \right|_{\xi=1} = - \frac{\zeta_d}{\alpha_1 \alpha_2 \beta} \left. \frac{\partial \overline{u}}{\partial \tau} \right|_{\xi=1}, \tag{64}$$

In (61) the scaled bit-rock interaction force is determined by

$$\overline{F}_b = \begin{cases} -\beta_b \overline{u}(0,t), & \overline{u}(0,t) < 0,\ \frac{\partial \overline{u}(0,t)}{\partial \tau} < 0 \\ \beta_b \overline{\delta}_m - \gamma' \beta_b \left[\overline{u}(0,t) + \overline{\delta}_m\right] = 0, & \overline{u}(0,t) < 0,\ \frac{\partial \overline{u}(0,t)}{\partial \tau} > 0, \\ 0, & \overline{u}(0,t) > 0 \end{cases} \tag{65}$$

with $\beta_b = k_b L/EA_1$ denoting the ratio between the stiffness of the bit-rock interface and that of the rod, and δ_m denoting the maximum $\overline{u}(0,t)$ during the loading process. The scaled continuity and initial conditions are given by:

$$\overline{u}(\xi_1^-, \tau) = \overline{u}(\xi_1^+, \tau) = \overline{u}(\xi_1, \tau) \tag{66}$$

$$\overline{u}(\xi_2^-, \tau) = \overline{u}(\xi_2^+, \tau) = \overline{u}(\xi_2, \tau) \tag{67}$$

$$\overline{u}(\xi, \tau) = 0, \qquad \frac{\partial \overline{u}(x,0)}{\partial t} = 0, \qquad \overline{U}(0) = 0, \qquad \dot{\overline{U}}(0) = 0 \tag{68}$$